Hindawi Publishing Corporation
Advances in Meteorology
Volume 2016, Article ID 1584316, 14 pages
http://dx.doi.org/10.1155/2016/1584316

Research Article

Satellite Retrieval of Surface Evapotranspiration with Nonparametric Approach: Accuracy Assessment over a Semiarid Region

Xin Pan,[1,2] Yuanbo Liu,[1] and Xingwang Fan[1]

[1]*Key Laboratory of Watershed Geographic Sciences, Nanjing Institute of Geography and Limnology, Chinese Academy of Sciences, 73 East Beijing Road, Nanjing 210008, China*
[2]*University of Chinese Academy of Sciences, 19 Yuquan Road, Beijing 100049, China*

Correspondence should be addressed to Yuanbo Liu; ybliu@niglas.ac.cn

Received 2 December 2015; Revised 7 March 2016; Accepted 18 April 2016

Academic Editor: Iftekhar Ahmed

Surface evapotranspiration (ET) is one of the key surface processes. Reliable estimation of regional ET solely from satellite data remains a challenge. This study applies recently proposed nonparametric (NP) approach to retrieve surface ET, in terms of latent heat flux (LE), over a semiarid region. The involved input parameters are surface net radiation, land surface temperature, near-surface air temperature, and soil heat flux, all of which are retrievals or products of the Moderate-Resolution Imaging Spectroradiometer (MODIS). Field observations are used as ground references, which were obtained from six eddy covariance (EC) sites with different land covers including desert, Gobi, village, orchard, vegetable field, and wetland. Our results show that the accuracy of LE retrievals varies with EC sites with a determination of coefficient from 0.02 to 0.76, a bias from −221.56 W/m^2 to 143.77 W/m^2, a relative error from 8.82% to 48.35%, and a root mean square error from 67.97 W/m^2 to 239.55 W/m^2. The error mainly resulted from the uncertainties from MODIS products or the retrieval of net radiation and soil heat flux in nonvegetated region. It highlights the importance of accurate retrieval of the input parameters from satellite data, which are the ongoing tasks of remote sensing community.

1. Introduction

Evapotranspiration (ET) includes evaporation from various land surfaces and transpiration from vegetation [1]. ET is interchangeable to the associated latent energy (LE) [2]. It is a key land surface process in regulating regional hydrological and climatic characteristics. As the only way back to the atmosphere, global land ET returns about 60% of annual land precipitation to the atmosphere [3]. Accurate estimation of ET is important for regional water resources management, especially in arid regions.

ET is intrinsically difficult to measure and predict especially at a large spatial scale. Various approaches are proposed to estimate ET in succession after the 18th century, including the Penman evaporation equation [4], the Penman-Monteith (P-M) combination equation [5], and the Priestley and Taylor approach [6]. Traditional measurement or estimation of LE is mostly applicable at a point-scale [7–9], including eddy covariance (EC) techniques [10]. However, representativeness of the point-scale measurement for a large area is generally problematic, and the dense coverage of point measurements is not feasible [11].

Alternatively, remote sensing technology can efficiently solve the representation limitation of the point measurement. However, it cannot observe LE directly, whereas it provides retrievals of geophysical parameters to estimate LE at a regional scale [12]. Several retrieval algorithms appeared in the last two decades [13, 14], including the triangle approach [15–17], the simplified surface energy balance index (S-SEBI) [18], the surface energy balance system (SEBS) [19], the three-temperature model [20–22], the MOD16 algorithm [23, 24], and other P-M remote sensing methods [25, 26]. They are widely applied to estimate regional or global ET from remotely sensed data [25–31]. The existing algorithms have

a relative error from 10% to 40% [32, 33] in their validation sites. For example, Gillies et al. [34] used aircraft scanner data and the tringle approach to retrieve LE in an area covered with grasslands, steppe-shrub, and tall-grass prairie. The LE retrievals had a root mean square error (RMSE) value of 22~55 W/m^2 and a relative error (RE) of 10%~30%, in reference to field measures by EC techniques and Bowen-radio approaches. Verstraeten et al. [28] used the advanced very high resolution radiometer (AVHRR) and the S-SEBI approach to retrieve LE in forestland. This achieved a RMSE (RE) of 35 W/m^2 (24%), compared to EC measures. Su [19] used the Moderate-Resolution Imaging Spectroradiometer (MODIS) data and the SEBS approach to estimate LE in wheat, corn, and rainforest areas. The LE retrievals had a RE of 25%, compared to EC measures. Xiong and Qiu [22] used the three-temperature approach and Landsat Thematic Mapper (TM) data to retrieve instantaneous LE in grassland and hills. Relative to Bowen ratio systems, LE had a RE of 4.65%~100% or 0.02~0.20 mm h^{-1} during the satellite overpassing time. Mu et al. [23] evaluated the MOD16 products and reported an average bias (RE) of 0.31 mm day^{-1} (24.1%) for daily ET at FLUXNET-EC sites. Zhang et al. [25] applied normalized difference vegetation index- (NDVI-) based ET algorithm to assess global terrestrial LE using AVHRR GIMMS NDVI data. The daily results had a favorable accuracy with RMSE of about 10~40 W/m^2 at 34 flux tower sites. Similarly, Leuning et al. [26] introduced a remotely sensed leaf area index- (LAI-) based P-M algorithm to calculate regional daily average evaporation using MODIS LAI products. At 15 flux sites globally, the systematic RMSE in daytime mean evaporation was in the range of 0.09~0.50 mm day^{-1}, whereas the unsystematic component was in the range of 0.28~0.71 mm day^{-1}.

A nonparametric approach (NP) has been recently proposed for estimating surface evapotranspiration [35]. It uses net radiation, surface air temperature, land surface temperature, and soil heat flux as the inputs, without the need of parameterizing surface resistance. All the necessary inputs are measurable, offering a novel but simple approach for practical use. The approach has been validated at 24 EC sites, yet it was not tested with remote sensing application. This paper applies the NP approach to estimate regional LE covering different surfaces, evaluates the accuracy of LE retrievals from MODIS data only, and identifies the error sources which are useful for improving retrieval accuracy.

2. Methodology

2.1. The Nonparametric Evapotranspiration Approach. Surface net radiation (R_n) is the net amount of radiation entering and leaving the Earth's surface. A part of R_n is transformed into surface soil heat flux (G_s), and another part controls LE and sensible heat flux (H_s). In NP approach, a homogeneous terrestrial ground surface layer is assumed for a macrostate system, and Hamiltonian (potential energy plus kinetic energy) is the total energy of this system. R_n serves as the potential energy, whereas G_s, H_s, and LE serve as kinetic energy. The land surface temperature (LST) serves as a generalized coordinate in this system. The approach calculates the partial differential equations of Hamiltonian with LST (T_s). The final forms are [35]

$$H_{T_s} = \frac{\gamma}{\Delta+\gamma}\left(R_n - G_s\right) + \varepsilon\sigma\left(T_s^4 - T_a^4\right) - G_s \ln\left(\frac{T_s}{T_a}\right),$$
$$\mathrm{LE}_{T_s} = \frac{\Delta}{\Delta+\gamma}\left(R_n - G_s\right) - \varepsilon\sigma\left(T_s^4 - T_a^4\right) + G_s \ln\left(\frac{T_s}{T_a}\right), \quad (1)$$

where ε is land surface emissivity (LSE), T_a is near-surface air temperature (AT), Δ is the slope of saturated vapor pressure at temperature T_a, γ is the psychometric constant, and σ is the Stefan-Boltzmann's constant (5.67×10^{-8} Wm^{-2} K^{-4}). γ can be estimated by the near-surface pressure (P).

2.2. Retrieval Algorithms for Net Radiation and Soil Heat Flux as Inputs to the NP Approach. Bisht's R_n retrieval algorithm [36] is simple and accurate to estimate instantaneous R_n over large heterogeneous areas under clear sky days. R_n is calculated in Bisht's algorithm:

$$R_n = (1-\alpha)\,R_{sd} + \varepsilon\sigma\left(\varepsilon_a T_a^4 - T_s^4\right),$$
$$R_{sd} = \frac{S_0 \cos^2\theta}{d},$$
$$d = 1.085\cos\theta + e_0\,(2.7 + \cos\theta) \times 10^{-3} + 0.1,$$
$$\varepsilon = 0.273 + 1.778\varepsilon_{31} - 1.807\varepsilon_{31}\varepsilon_{32} - 1.037\varepsilon_{32} + 1.774\varepsilon_{32}^2, \quad (2)$$
$$\varepsilon_a = \left[1 - \left(1 + \frac{46.5 e_0}{T_a}\right)\exp\left\{-\left(1.2 + 3\cdot\frac{46.5 e_0}{T_a}\right)^{1/2}\right\}\right],$$
$$e_0 = 6.11 \exp\left[\frac{L_v}{R_v\left(1/273 - 1/T_d\right)}\right],$$

where S_0 is the solar constant at the top of the atmosphere (about 1367 W/m^2), α is the surface albedo, θ is the solar zenith angle (SZA), e_0 is the water vapor pressure, ε_a is the air emissivity, and ε_{31} and ε_{32} denote the emissivity in bands 31 and 32 of MODIS, respectively. R_{sd} is the downwell shortwave radiation. L_v is the latent heat of vaporization (2.5×10^6 J/kg), R_v is the gas constant for water vapor (461 J kg^{-1} K^{-1}), and T_d is the dew point temperature at screen level. For the surface albedo, it is derived by the following equation [37]:

$$\alpha = 0.160\alpha_1 + 0.291\alpha_2 + 0.243\alpha_3 + 0.116\alpha_4 + 0.112\alpha_5 + 0.081\alpha_7, \quad (3)$$

where α_1, α_2, α_3, α_4, α_5, and α_7 are the nadir BRDF-adjusted albedos in bands 1, 2, 3, 4, 5, and 7 of MODIS, respectively.

At long time scales, G_s is commonly assumed to be negligible. But at subdaily scale, the G_s varies with the time

of day, and the values of G_s are not always negligible. It can be parameterized with the following equation [38]:

$$G_s = 0.583 \exp(-2.13\text{NDVI})\, R_n. \quad (4)$$

Obviously, G_s is regarded as a function of normalized difference vegetation index (NDVI) and R_n.

2.3. Correction of EC Measures Used as Reference for Accuracy Assessment. Although EC is the most accurate technique to measure the turbulent fluxes of sensible and latent heat, the energy balance can not be closed with EC data at the Earth surface with a closure of the energy balance of approximately 80% [39, 40]. In addition, relative to the fluctuations of LE accuracy, H_s is measured in more reliable accuracy [41–43]. So it is necessary to correct LE directly measured by EC for validation.

A preferred method can be derived from energy balance [44, 45]. On the large-scale homogeneous surface and steady-state condition, the corrected LE (ERLE) is

$$\text{ERLE} = R_n - G_s - H_{EC}, \quad (5)$$

where H_{EC} is H_s measured by EC. The ERLE is the reference of validation for remote sensing retrieved LE (RSLE).

2.4. Metrics for Accuracy Assessment. The linear regression approach is used to describe the accordance between RSLE and ERLE. The determination of coefficient (R^2), slope, and intercept of the linear fit between RSLE and ERLE are subsequently obtained. The accordance is more satisfactory when the regression line is nearer to 1 : 1 line and R^2 is higher.

Their definitions are described as follows [46]:

$$R^2 = 1 - \frac{\sum_{i=1}^{n} (s_i - o_i)^2}{\sum_{i=1}^{n} (s_i - \overline{o})^2},$$

$$\text{Slope} = \frac{\sum_{i=1}^{n} s_i \cdot (o_i - \overline{o})^2}{\sum_{i=1}^{n} (o_i - \overline{o})^2}, \quad (6)$$

$$\text{Intercept} = \frac{\sum_{i=1}^{n} (s_i - \text{Slope} \cdot o_i)}{n},$$

where s_i means retrieve values, o_i means reference values, $\overline{o}$ means the average of o_i, $i = 1, \ldots, n$, and n is the number of pair data for comparison.

In addition, bias, relative error (RE), and RMSE are used to quantify errors of RSLE. Bias quantifies the average absolute difference between retrieve values and reference values. RE is the absolute value of the bias divided by the magnitude of the reference values. RMSE is the standard deviation of the retrieve values around reference values. Basically, the RMSE represents a combination of standard deviation and bias.

Their definitions are described as follows [47]:

$$\text{Bias} = \frac{\sum_{i=1}^{n} (s_i - o_i)}{n},$$

$$\text{RE} = \frac{|\text{Bias}|}{(1/n) \sum_{i=1}^{n} o_i} \times 100\%, \quad (7)$$

$$\text{RMSE} = \sqrt{\frac{\sum_{i=1}^{n} (s_i - o_i)^2}{n}}.$$

3. Study Materials and Data Processing

3.1. Study Area and Ground Sites. As a typical inland river basin in the northwest of China, the Heihe River Basin is located between 97°24′~102°10′E and 37°41′~42°42′N and covers an area of approximately 130 000 km^2. The selected 6 ground observation sites are parts of multiscale EC observation matrices belonging to Heihe Watershed Allied Telemetry Experimental Research (HiWATER) [48, 49], and they are acquired over the Zhangye region (100°25′E, 38°51′N, 1519 m) in the middle reaches of Heihe River Basin (Figure 1). A total of 6 EC sites measuring LE and H_s are used for data analysis and accuracy assessment (Table 1), accompanied by 6 automatic weather stations (AWS) which are used to measure the near-surface meteorological parameters. In view of spatial homogeneity and underlying representativeness, observations focus on six different areas with landscapes ranging from moist vegetated surfaces (vegetable, orchard, and wetland) to arid nonvegetated surfaces (village, desert, and Gobi). The locations of sites imply the similar climatic conditions. The underlying surfaces are homogeneous at all sites excepted for orchard and village sites. Based on the field visit, the fruit trees grow with bean seeding at orchard site. At village site, the underlying surface is composed of the bare soil, house, road, and trees.

All instruments were intercompared over the Gobi between 14 and 24 May, 2012 [43]. The intercompared and well agreed instruments, accompanied by the uniform data processing steps and standards, ensured data consistency, which guaranteed the reliability of validation [50]. All selected sites were covered by different land cover types. Thus, for convenience, the site names were replaced by the types of underlying surfaces here.

3.2. Data Description

3.2.1. Meteorological and Surface Flux Data. Acquired from the HiWATER, the EC and AWS data span from June 25 to September 15 in 2012, the overlapping time span of EC data at all sites (Table 2). All AWS and EC data were produced, archived, and made available to the scientific community by the Cold and Arid Regions Science Data Center at Lanzhou [43, 51]. They were used for validation and error source analysis of RSLE. All LE validation references were obtained by H_s (directly measured by EC), R_n, and G_s (measured by AWS) (see (5)).

The parameters obtained by AWS were averaged every 10 minutes, whereas the temporal resolution of EC was 30

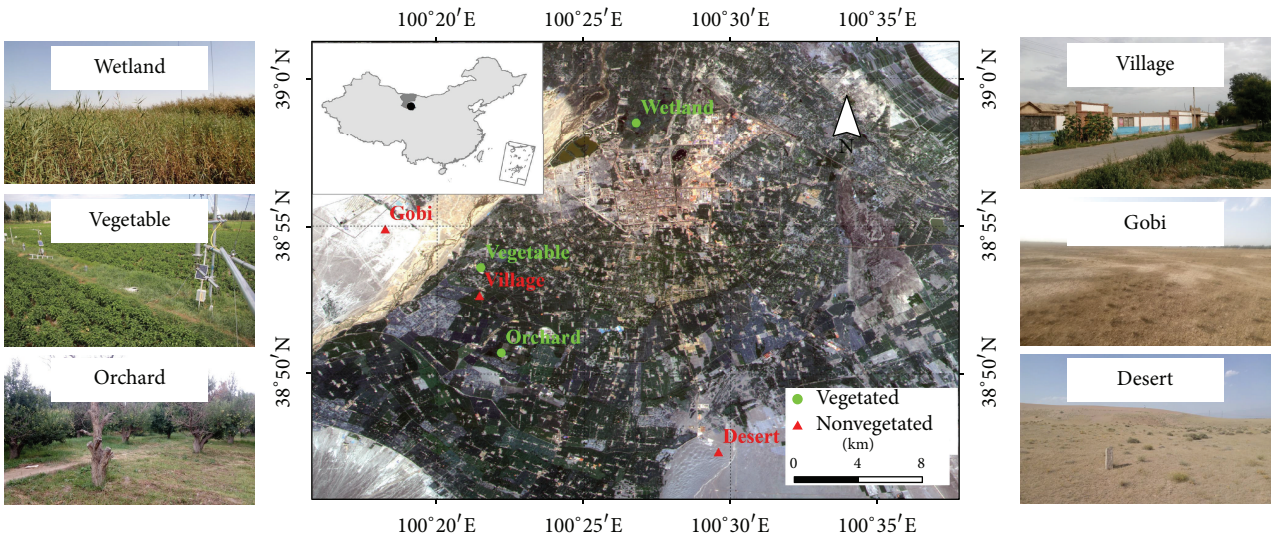

Figure 1: Geolocation of EC observation sites and illustration of land surface.

Table 1: Descriptive information of EC sites.

Type	Sites	Longitude (°)	Latitude (°)	Altitude (m)	EC height (m)
Vegetated	Wetland	100.446	38.975	1460	5.2
	Vegetable	100.358	38.893	1552	3.8
	Orchard	100.370	38.845	1559	7.0
Nonvegetated	Village	100.358	38.878	1561	4.2
	Gobi	100.304	38.915	1562	4.6
	Desert	100.493	38.789	1594	4.6

Table 2: Datasets for analysis.

Datasets	Parameters	Temporal-spatial resolution	Data types	Data purpose
EC	LE/H_s	30 minutes, hundreds of meters	Meteorology	Validation
AWS	$P/R_{ld}/R_{lu}/T_a/R_n/G_s$	10 minutes, several meters to hundreds of meters	Meteorology	Validation
ASTER	ε	10–20 days, 90 m	Remote sensing	Validation
MYD07	$P/T_d/T_a/\theta$	Daily, 5 km	Remote sensing	Retrieval
MCD43	α	8 days, 1 km	Remote sensing	Retrieval
MYD11	T_s/ε	Daily, 1 km	Remote sensing	Retrieval
MYD13	NDVI	16 days, 1 km	Remote sensing	Retrieval

minutes. So we need to average the parameters derived from AWS to the mean in 30 minutes. In addition, consider that the time of satellite overpassing, AWS, and EC data at the nearest moment were regarded as the actual values of input parameters. Except for LST, other actual values were measured directly by AWS. The actual LST was estimated from the upwelling and downwelling longwave radiation measured by AWS using the following equation:

$$T_s = \left[\frac{R_{lu} - (1-\varepsilon)\cdot R_{ld}}{\varepsilon \cdot \sigma}\right], \quad (8)$$

where R_{lu} (R_{ld}) is the surface upwelling (downwell) longwave radiation.

3.2.2. Remote Sensing Data. Remote sensing data were obtained from the MODIS and Advanced Spaceborne Thermal Emission and Reflection Radiometer (ASTER) products. The pixels located at the sites were obtained to retrieve LE. All chosen images were acquired under clear sky during 13:00 to 15:00 (local time) from June 25 to September 15, 2012. The temporal and spatial resolutions of these products were listed in Table 2.

MODIS are onboard NASA's Earth Observation System TERRA and AQUA satellites [52]. As mentioned above, various products (MOD, MYD, and MCD) are provided by MODIS. They have been produced, archived, and made available to the scientific community by the Level 1 and

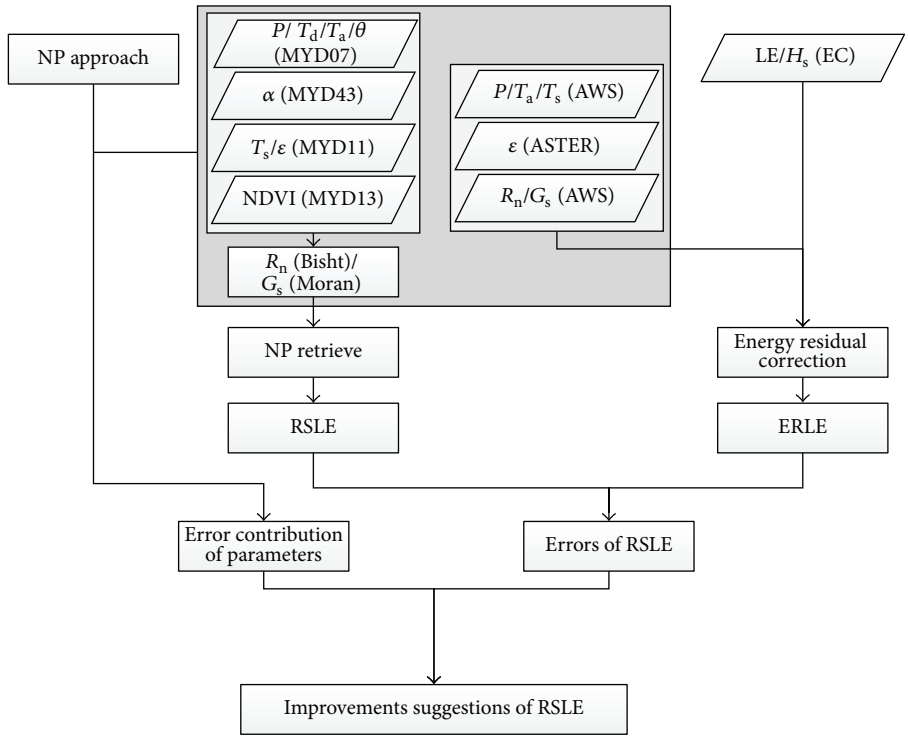

Figure 2: Schematic representation of the procedure for analysis in our study.

Atmosphere Archive and Distribution System (LAADS), the National Aeronautics and Space Administration (NASA). In our study, both MYD and MCD (MYD07, MYD11, MYD13, and MCD43) were selected to retrieve LE. MYD07 provided the profile of air temperature and moisture to obtain the near-surface atmospheric temperature and dew temperature [53]. MYD11 provided the land surface temperature and emissivity [54]. MYD13 provided the 16-day NDVI [55, 56]. MCD43 provided 8-day nadir BRDF-adjusted albedos [57, 58], including the albedo in band 1 to band 7.

ASTER radiometer has 5 thermal infrared (TIR) bands to provide TIR spectral emissivity variations at 90 m spatial resolution [59]. LSE product is produced by the Temperature and Emissivity Separation (TES) algorithm [60]. In our study, ASTER product was also provided by the Cold and Arid Regions Science Data Center at Lanzhou [61, 62]. ASTER product was used to estimate LSE. LSE can be represented by the ASTER narrowband emissivities using the following linear equation [63]:

$$\varepsilon = 0.197 + 0.025\varepsilon_{10} + 0.057\varepsilon_{11} + 0.237\varepsilon_{12} + 0.333\varepsilon_{13} + 0.146\varepsilon_{14}, \quad (9)$$

where ε_{10}~ε_{14} are the five ASTER narrowband emissivities. It was regarded as the real value of LSE because of the high accuracy and spatial resolution.

3.3. Data Processing. Aiming to ascertain the applicability of LE retrieve algorithm, the validation and error source analysis of RSLE were made at the different sites (Figure 2). Firstly, the LE obtained by EC was corrected by R_n, G_s (obtained by AWS), and H_s (obtained by EC) in the way of energy residual correction (see (5)). Secondly, R_n and G_s were retrieved by MODIS product in Bisht's and Moran's algorithm ((2) and (4)), respectively. Then, RSLE can be estimated in NP approach (see (1)). The errors of RSLE were derived from the discrepancies between RSLE and ERLE. Thirdly, to qualify the error contribution due to the input error of one parameter, that parameter (derived from MODIS) and the other actual parameters (measured by AWS/ASTER) were brought in NP approach to get LE estimation (see (1)). Similarly, all actual input parameters (measured by AWS/ASTER) were bought in NP approach to get LE estimation, too. The difference among these two estimations was regarded as the error contribution of the parameter at the retrieval moment [64]. Fourthly, according to the error analysis, we searched for the probable ways to improve the retrieve accuracy.

4. Results

4.1. Data Features at the Sites. Table 3 showed energy fluxes and environmental parameters measured by surface observations at the six sites. In the order of decreasing surface moistures, these sites were listed as wetland, vegetable, orchard, village, Gobi, and desert sites. The decreasing order matched pretty well with the vegetation abundances at these sites. Generally, there were higher LE in vegetated region with higher R_n/LSE and lower G_s/LST. In detail, R_n was higher at vegetated than nonvegetated sites. Mean amount of R_n was 625~735 W/m^2 for vegetated sites, and it decreased to

Table 3: Average of fluxes and environment parameters derived from AWS/ASTER at the six sites in the EC matrices, including net radiation (R_n), soil heat flux (G_s), land surface temperature (T_s), near-surface air temperature (T_a), land surface emissivity (LSE), near-surface pressure (P), latent heat (LE), and sensible heat (H_s). The energy residual corrected (ER) LE is also revealed.

Parameters	Types	Wetland	Vegetable	Orchard	Village	Gobi	Desert
R_n (W/m^2)	AWS	625.12	646.55	735.09	543.48	489.84	519.40
G_s (W/m^2)	AWS	96.39	64.34	62.35	86.95	90.06	90.40
T_s (K)	AWS	305.35	304.08	301.20	315.46	316.68	320.71
T_a (K)	AWS	299.78	299.18	298.72	300.02	298.29	299.58
LSE	ASTER	0.981	0.978	0.980	0.975	0.958	0.932
P (kpa)	AWS	89.11	88.32	83.89	83.28	84.02	84.10
LE (W/m^2)	ER	496.51	482.68	575.93	297.33	184.96	212.54

Table 4: Average of input parameters derived by MODIS products at the six sites, including land surface temperature (T_s), near-surface air temperature (T_a), land surface emissivity (LSE), near-surface pressure (P), dew point temperature (T_d), albedo, and NDVI. The retrieved net radiation (R_n), soil heat flux (G_s), and latent heat flux (LE) are also shown.

Parameters	Wetland	Vegetable	Orchard	Village	Gobi	Desert
T_s (K)	301.64	301.39	301.46	300.73	307.61	309.33
LSE	0.965	0.972	0.973	0.973	0.964	0.963
P (kpa)	79.80	78.73	77.96	78.47	79.15	77.06
T_d (K)	277.33	279.07	279.35	279.55	278.28	278.08
T_a (K)	298.15	298.58	291.75	296.16	299.10	289.44
Albedo	0.193	0.171	0.171	0.165	0.207	0.186
NDVI	0.713	0.701	0.717	0.790	0.143	0.117
R_n (W/m^2)	654.26	685.18	650.64	685.19	616.08	572.75
G_s (W/m^2)	84.46	89.46	83.35	73.91	264.77	257.16
LE (W/m^2)	425.07	452.25	354.37	441.10	233.28	120.48

490~540 W/m^2 for nonvegetated sites. The difference was probably due to high surface albedo at nonvegetated sites. G_s increased from vegetated (down to 62.34 W/m^2 for vegetable) to nonvegetated sites (up to 90.40 W/m^2 for desert). After energy residual correction, ERLE was higher at vegetated sites (483~576 W/m^2) than at nonvegetated sites (185~297 W/m^2). Mean LSE was in the range of 0.978~0.981 and 0.932~0.975 for vegetated and nonvegetated sites. On the contrary, LST was considerably lower at vegetated sites with typical values of 300~305 K, compared to 315~320 K at nonvegetated sites. The near-surface pressure was higher at vegetated sites than at nonvegetated sites (up to 89.11 kpa for wetland, and down to 83.28 kpa for desert). The difference of AT was little, and there was about 299 K of AT at all sites. These environmental parameters were the background of LE retrieve.

4.2. MODIS Retrievals of R_n, G_s, and LE. R_n, G_s, and LE were all derived from satellite retrieve. Table 4 showed input parameters obtained by satellite retrieve at the six sites. The dew point temperature, pressure, and LSE were similar among all sites, with values of about 278 K, 78 kpa, and 0.96, respectively. Other parameters were different among sites. In detail, AT were 296~299 K at all sites except for orchard (292 K) and desert (289 K) sites. Low LST appeared at vegetated sites (about 301 K), whereas high LST occurred at nonvegetated sites (300~309 K). Similarly, albedo was slightly lower at vegetated sites with value of about 0.17, compared to about 0.19 at nonvegetated sites. Thus, generally, the retrieved R_n was higher in vegetated region (650~685 W/m^2) than in the nonvegetated region (570~685 W/m^2). Considering the lower NDVI at nonvegetated sites (less than 0.2), the higher retrieved G_s (more than 250 W/m^2) appeared there. On the basis of the retrieved R_n and G_s, RSLE was higher at vegetated sites (350~450 W/m^2) than at the nonvegetated sites (120~440 W/m^2).

The instantaneous retrieve results of R_n, G_s, and LE in a part of Zhangye region at 05:55 (UTC) in August 20, 2012, were shown in Figure 3. The distribution of LE, R_n, and G_s was in good accordance with the oasis-desert ecosystem. The desert (the east and south of the region) had lower R_n because of the high albedo here. The desert also had higher G_s because of bare surface. In addition, the oasis (the middle of the region) and wetland (the north of the region) had more evaporation than desert because of the irrigation. In view of retrieve values, the LE was up to 300~400 W/m^2 in the region of oasis, whereas the LE decreased to 150~250 W/m^2 in the region of desert. In general, the distribution of retrieve results was deemed to be reliable.

4.3. Accuracy Assessment of MODIS-Retrieved LE. Figure 4 revealed the relationship between ERLE (donated by x-axis) and RSLE (donated by y-axis) at the retrieval moment. In general, relative to ERLE in 30 minutes, the RSLE was generally accurate and underestimated with bias, RMSE, RE,

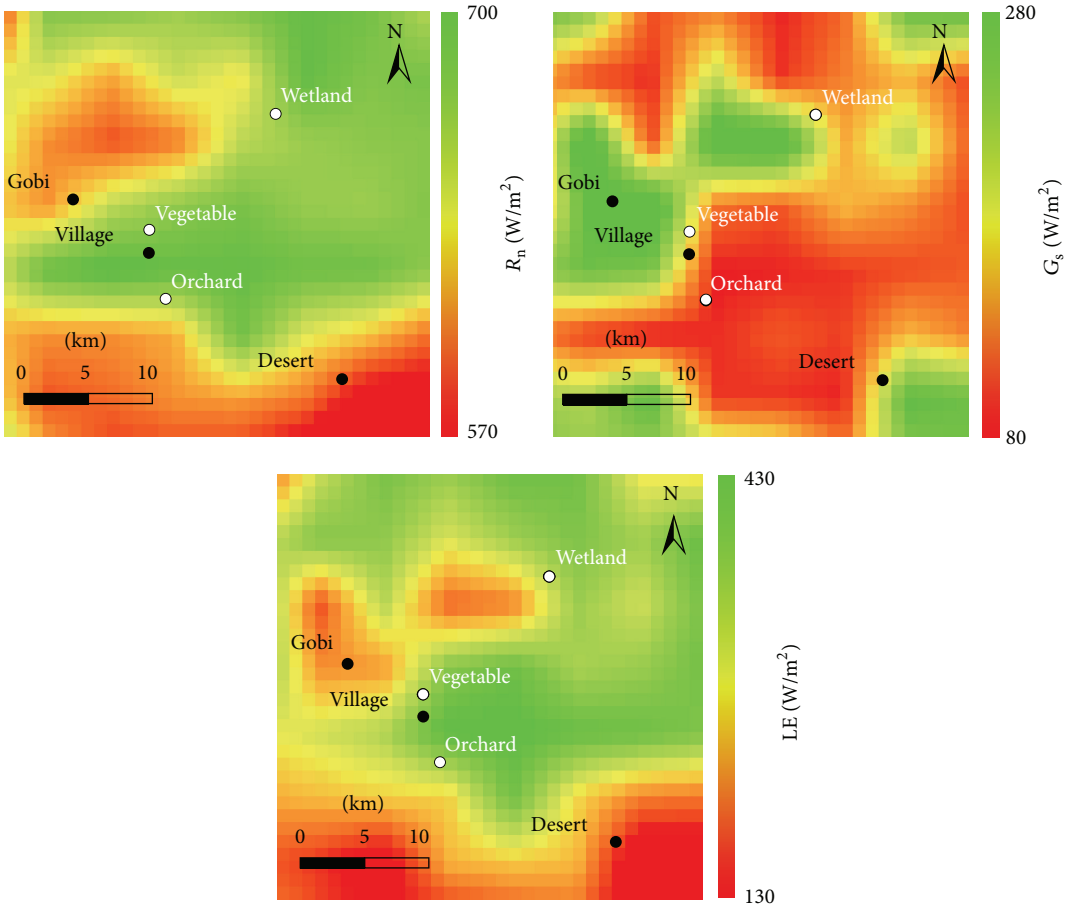

Figure 3: Distributions of the retrieved net radiation (R_n), soil heat flux (G_s), and latent heat flux (LE) in a part of Zhangye region at 05:55 (UTC) in August 20, 2012.

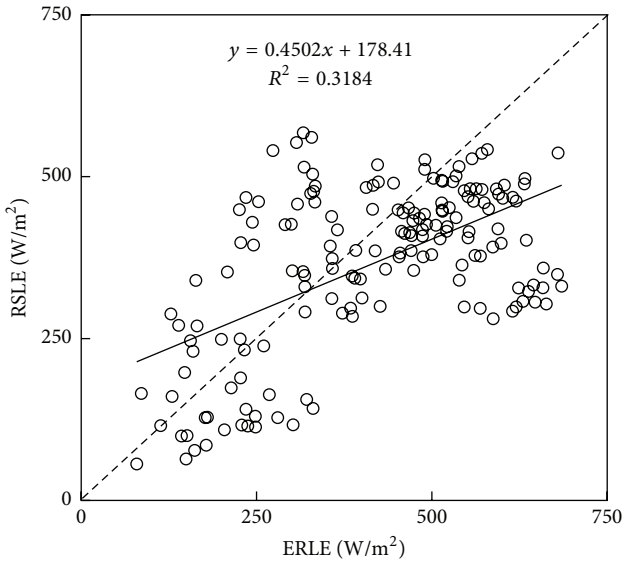

Figure 4: Overall comparison between ERLE and RSLE.

Table 5: Errors of RSLE at 6 sites; statistics include the bias, RMSE, and RE.

Sites	Bias (W/m^2)	RMSE (W/m^2)	RE (%)
Wetland	−71.44	79.77	14.39
Vegetable	−43.77	73.62	8.82
Orchard	−221.56	239.55	38.47
Village	143.77	160.14	48.35
Gobi	48.33	67.97	26.13
Desert	−92.32	105.64	43.44
Overall	*−49.64*	*144.20*	*11.97*

slope, and R^2 of −49.64 W/m^2, 144.20 W/m^2, 11.97%, 0.45, and 0.32, respectively (Table 5).

At the site scale, Figure 5 also showed the comparison between RSLE and ERLE at all 6 sites. RSLE was generally underestimated, and it was in relatively good agreement with ERLE at most of the sites, with R^2 of 0.11~0.76, bias of −222~49 W/m^2, RE of 9~49%, and RMSE of 68~240 W/m^2. The highest accuracy occurred at vegetable, wetland, and Gobi sites, with RE (RMSE) value of 8.82% (73.62 W/m^2), 14.39% (79.77 W/m^2), and 26.13% (67.97 W/m^2), respectively. The RSLE was less satisfactory at orchard and village sites, with RE of about 40~50% and RMSE of more than 160 W/m^2.

To validate the retrieved LE further, the LE directly observed by EC (ECLE) was also compared with RSLE in Figure 6. Similarly, the RSLE was in relatively good agreement with ECLE with R^2 of 0.11~0.36 at vegetated sites. Nevertheless, at the nonvegetated sites, the accordance disappeared with R^2 of 0.05~0.23. Relative to the ECLE in Figure 6, the ERLE matched better with retrieved surface LE in Figure 5, especially at nonvegetated sites. Thus, at least, the RSLE had a satisfactory accuracy at vegetated sites, and it also probably had a relatively good accuracy at nonvegetated sites.

4.4. Error Sources and Their Contributions to MODIS-Retrieved LE. To reveal the error contributions of input error, the input error of each parameter was showed firstly (Figure 7). R_n was retrieved with low accuracy at village, orchard, and Gobi sites with bias value of more than 80 W/m^2. There was a low accuracy of retrieved G_s at almost all sites, especially at Gobi and desert sites (bias values of about 170 W/m^2). The large difference (about 10 kpa) of surface pressure appeared at Gobi and desert sites. At most sites, the biases of AT were 2~5 K, except for orchard (−7 K) and desert (−10 K) sites. Similarly, the biases of LST were also 0~4 K at vegetated sites, whereas they were more than 9 K at nonvegetated sites. The LSE difference between MODIS and ASTER products was less than 0.01 at all sites except for Gobi (−0.036) and desert sites (0.031).

On the basis of input errors, the error contribution can be revealed. Figure 8 showed the error contributions of each factor (shown as the line) and the error of RSLE (shown as the columns) at 6 sites. Except for orchard and village sites, the RSLE were in relatively satisfactory accuracy, and the biases were within −90~50 W/m^2 at the other 4 sites. Based on the analysis of error sources, it was clear that the major error sources (inducing more than 40 W/m^2 RSLE error) were R_n, G_s, LST, and AT at nonvegetated sites, with error contributions of 40~110 W/m^2, −120~10 W/m^2, >60 W/m^2, and −100~10 W/m^2, respectively. At vegetated sites, input errors were not the dominant error sources of RSLE.

In detail, the large G_s error contribution (causing more than 100 W/m^2 RSLE error) appeared at Gobi and desert sites. About 100 W/m^2 RSLE error caused by the R_n error occurred at village and Gobi sites. The influence of AT and LST error on LE error was below 40 W/m^2 at most of sites, except for the LST at village and Gobi sites, the AT and LST at desert site, and AT at orchard site. The error contribution of LSE accounted for RSLE error as a small part (leading to less than 10 W/m^2 LE error). Similarly, the input errors of pressure affected RSLE error quite little (mostly less than 1 W/m^2). In addition, according to validation, the accuracy of RSLE was unsatisfactory at orchard and village with a bias of −221.56 W/m^2 and 143.77 W/m^2, respectively. At these two sites, the main errors sources (inducing more than 100 W/m^2 RSLE error) were AT and R_n.

5. Discussion

The improvement of input data can possibly benefit LE retrieve in the future. R_n and G_s are not the direct input parameters of algorithms but the indirect parameters retrieved by Bisht's and Moran's algorithm [36, 38]. The improvement of R_n and G_s retrieval algorithms is helpful to the improvement of RSLE. In our study, the Bisht's algorithm under clear sky [36] is selected as R_n retrieval algorithm. Considering the widespread cloud, Bisht's algorithm under all sky [65] can be chosen to broaden applications. Besides, the accuracy of retrieved R_n is especially unsatisfactory in arid nonvegetated region [36]. It is suitable to replace the retrieved R_n by the observation directly measured by the Clouds and the Earth's Radiant Energy System (CERES) project [66]. CERES's accuracy meets the demand of R_n input in the region of desert [67, 68]. For G_s, because of the subtle temporal variation of NDVI in the arid region, G_s retrieved by Moran's algorithm varies slightly. Thus, some more sensitive algorithm can be chosen for G_s, such as the G_s retrieval algorithm in SEBS model or in the way of thermal inertia [19, 27].

AT and the dew point temperature are derived from the atmospheric profile data of MYD07 in our study. They are not the values at the near-surface but the values of the atmospheric profile nearest to the surface. It is evident that the more accurate atmospheric information contributes to the retrieve of R_n and LE. So the other Earth observations with the high accuracy (e.g., the Goddard Earth Observing System Model, Version 5 (GEOS-5)) are optional substitutions [69]. For LST and LSE, they are derived from the MYD11 in the split-windows algorithm [54]. Wan et al. [70] have reported that just the average of bands 31 and 32 emissivities could lead to an overestimation of LSE, especially in arid and semiarid region. Accordingly, LST is underestimated in these regions. The MYD21 C6 is estimated to be published in 2016, and it can supply the more accurate LST and LSE based on TES algorithm [71], especially in the arid and semiarid region. That means the remarkable improvement of R_n and LE retrieve if we replace MYD11 by MYD21.

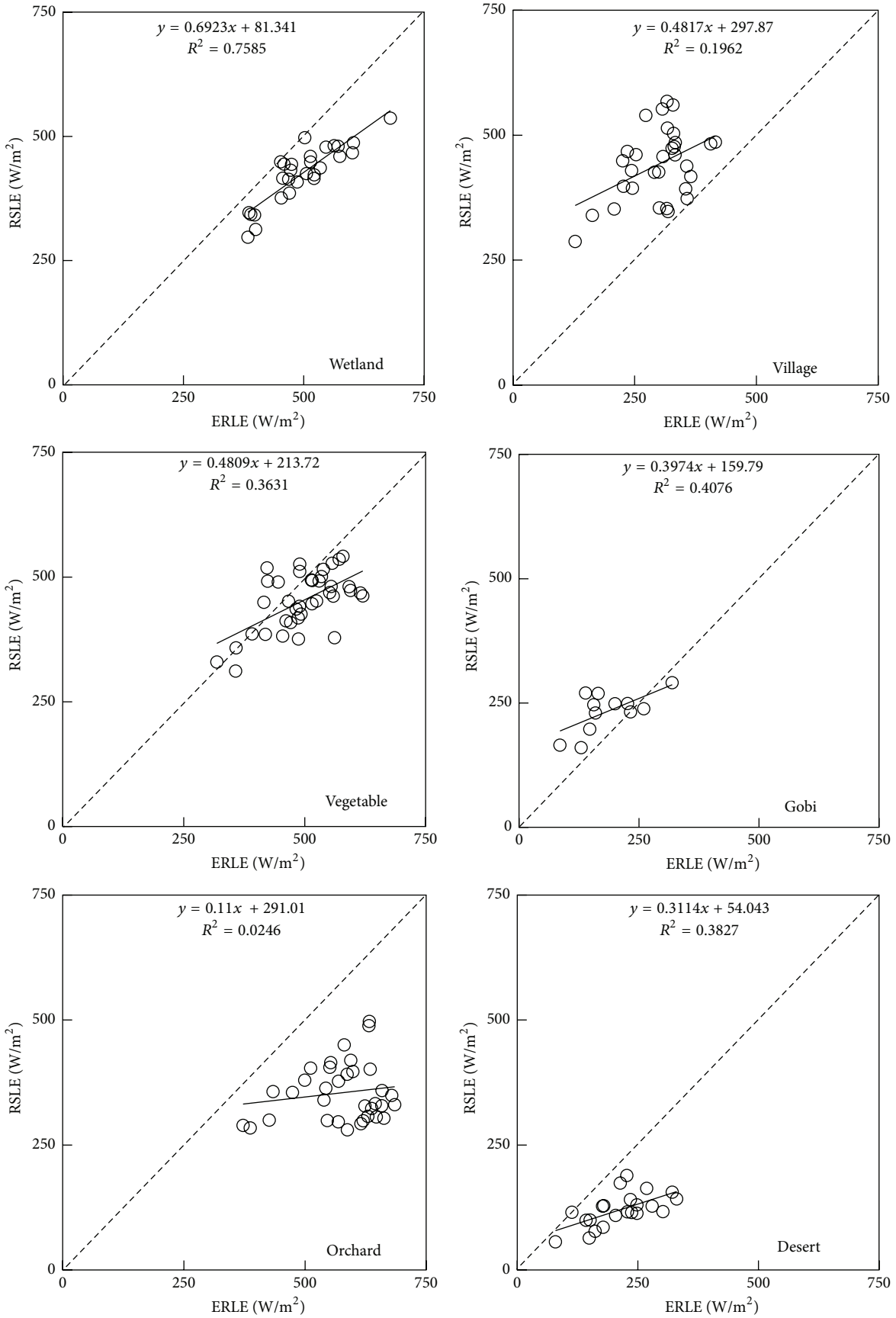

Figure 5: Comparisons between ERLE and RSLE at 6 sites.

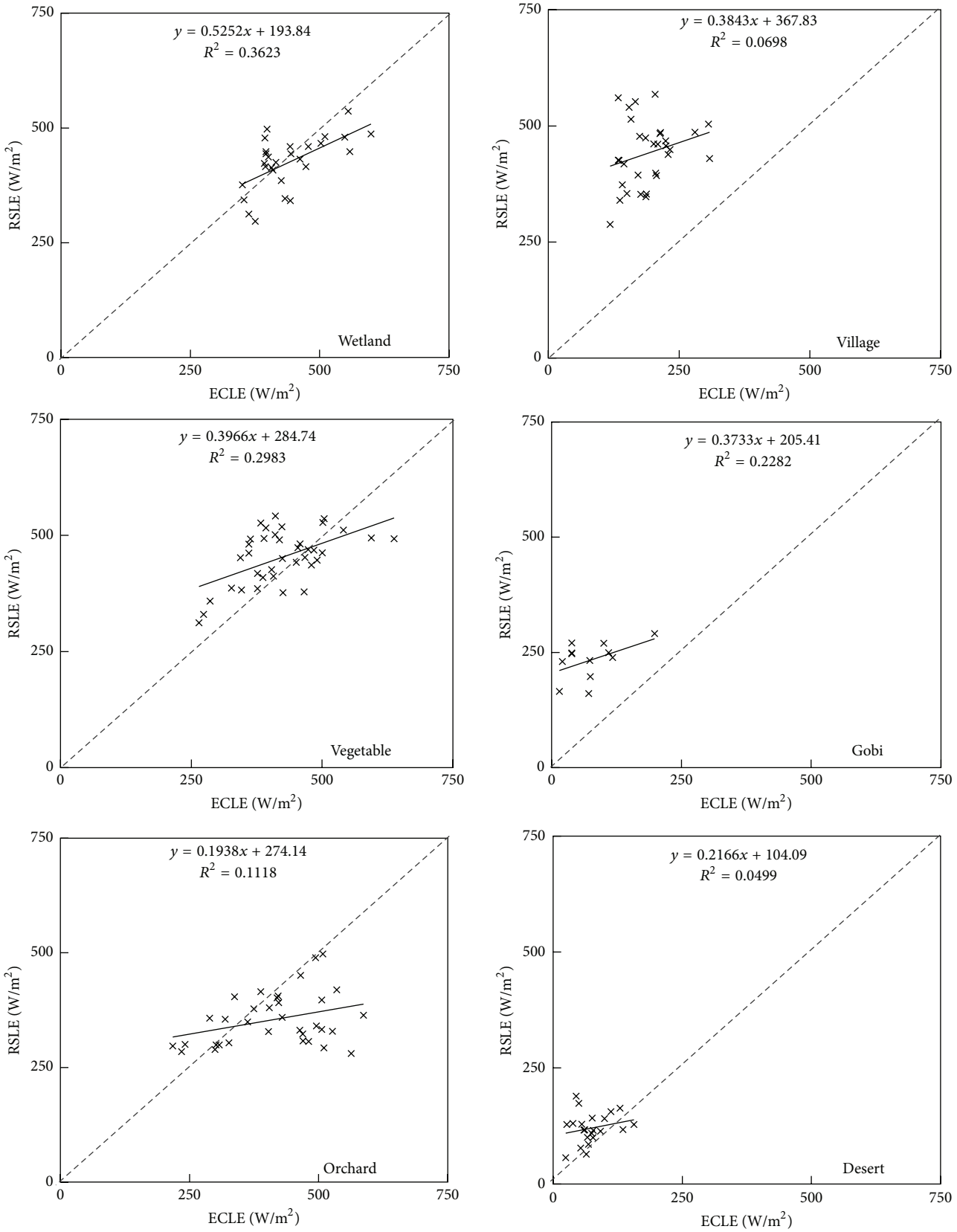

Figure 6: Comparisons between ECLE and RSLE at 6 sites.

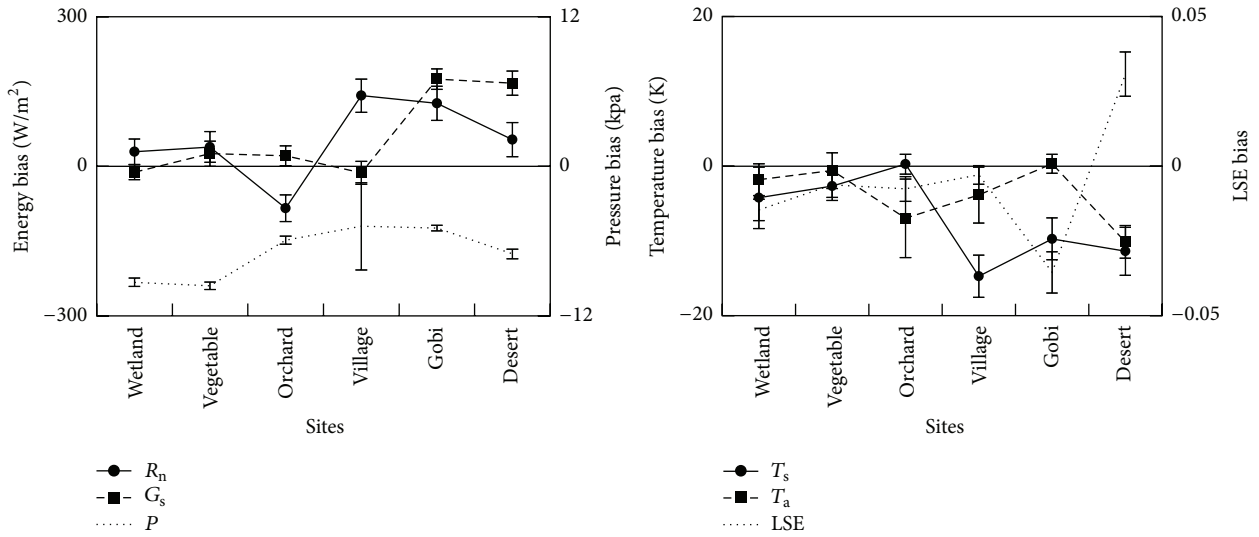

FIGURE 7: Average (line) and standard deviation (bar) of input parameter errors at 6 sites, including net radiation (R_n), soil heat flux (G_s), land surface temperature (T_s), near-surface air temperature (T_a), land surface emissivity (LSE), and near-surface pressure (P).

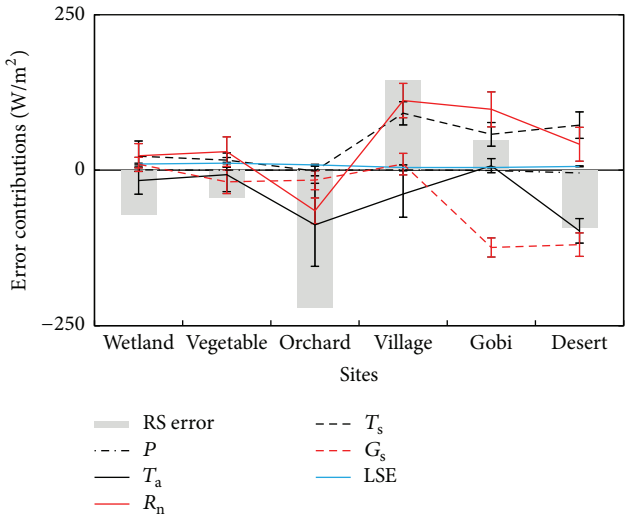

FIGURE 8: Error contributions of each factor, including the averages (line) and standard deviation (bar), along with errors of RSLE (column).

Other datasets with a higher spatial and temporal resolution can be also used to retrieve LE, such as NDVI and albedo products. In our study, the NDVI/albedo is assumed to be invariant in 16/8 days. There is a way to improve the temporal consistency by using other NDVI and albedo products with 1 km and 5-day resolution [72–74]. Furthermore, the correction based on digital elevation models should be considered in the region with undulant surfaces [31, 75].

6. Conclusions

NP approach provides a novel but simple method to estimate LE. In our study, NP approach attempts to develop a LE retrieval algorithm under clear sky which primarily uses remote sensing information and eliminates the need for ground information as model input, by using various land and atmospheric data products available from MODIS. The validation of retrieval result and the exploration of error sources were analyzed in succession.

At the temporal and spatial scales, the result of RSLE is within a reliable range. At the retrieve moment, RSLE is generally accurate. The instantaneous RSLE is underestimated with bias, R^2, RE, and RMSE values of −49.64 W/m^2, 0.32, 11.97%, and 144.20 W/m^2, respectively. At the site scale, RSLE is in relatively good accuracy at all sites, with R^2 = 0.11~0.76, bias = −222~49 W/m^2, RE = 9~49%, and RMSE = 68~240 W/m^2. Nevertheless, the accuracy of RSLE is unsatisfactory at orchard and village sites. In view of error source, in arid nonvegetated region, the dominant error contributions (causing 40 W/m^2 error of RSLE) are R_n, G_s, LST, and AT. In vegetated region, the input errors are not the dominant error sources of RSLE. In order to improve the accuracy of RSLE, some improvement recommendations of input parameters can be considered in the future. The future research work would aim to improve the accuracy of LE estimation.

Competing Interests

The authors declare that they have no competing interests.

Acknowledgments

This work is supported by the National Natural Science Foundation of China (no. 91125004). The authors thank the Cold and Arid Regions Science Data Center at Lanzhou for providing observation data (http://westdc.westgis.ac.cn) and the LAADS for providing MOIDS products (http://ladsweb.nascom.nasa.gov). They also thank Professor Liu S. M. and

Dr. Xu Z. W. for their kind assistance in providing field data and help in field visit.

References

[1] R. Burman and L. O. Pochop, *Evaporation, Evapotranspiration and Climatic Data*, Elsevier Science, Amsterdam, The Netherlands, 1994.

[2] W. Brutsaert, *Evaporation into the Atmosphere: Theory, History, and Applications*, Springer, Dordrecht, The Netherlands, 1982.

[3] T. Oki and S. Kanae, "Global hydrological cycles and world water resources," *Science*, vol. 313, no. 5790, pp. 1068–1072, 2006.

[4] H. L. Penman, "Natural evaporation from open water, bare soil and grass," *Proceedings of the Royal Society A: Mathematical, Physical and Engineering Sciences*, vol. 193, no. 1032, pp. 120–145, 1948.

[5] J. L. Monteith, "Evaporation and environment," *Symposia of the Society for Experimental Biology*, vol. 19, pp. 205–234, 1965.

[6] C. H. Priestley and R. J. Taylor, "On the assessment of surface heat flux and evaporation using large-scale parameters," *Monthly Weather Review*, vol. 100, no. 2, pp. 81–92, 1972.

[7] T. A. Howell, A. D. Schneider, D. A. Dusek, T. H. Marek, and J. L. Steiner, "Calibration and scale performance of Bushland weighing lysimeters," *Transactions of the American Society of Agricutural Engineering*, vol. 38, no. 4, pp. 1019–1024, 1995.

[8] M. Ibáñez and F. Castellví, "Simplifying daily evapotranspiration estimates over short full-canopy crops," *Agronomy Journal*, vol. 92, no. 4, pp. 628–632, 2000.

[9] D. A. Zeweldi, M. Gebremichael, J. Wang, T. Sammis, J. Kleissl, and D. Miller, "Intercomparison of sensible heat flux from large aperture scintillometer and eddy covariance methods: field experiment over a homogeneous semi-arid region," *Boundary-Layer Meteorology*, vol. 135, no. 1, pp. 151–159, 2010.

[10] D. Baldocchi, E. Falge, L. Gu et al., "FLUXNET: a new tool to study the temporal and spatial variability of ecosystem-scale carbon dioxide, water vapor, and energy flux densities," *Bulletin of the American Meteorological Society*, vol. 82, pp. 2415–2434, 2001.

[11] B. Mueller, S. I. Seneviratne, C. Jimenez et al., "Evaluation of global observations-based evapotranspiration datasets and IPCC AR4 simulations," *Geophysical Research Letters*, vol. 38, no. 6, Article ID L06402, 2011.

[12] K. Wang and R. E. Dickinson, "A review of global terrestrial evapotranspiration: observation, modeling, climatology, and climatic variability," *Reviews of Geophysics*, vol. 50, no. 2, Article ID RG2005, 2012.

[13] D. Courault, B. Seguin, and A. Olioso, "Review on estimation of evapotranspiration from remote sensing data: from empirical to numerical modeling approaches," *Irrigation and Drainage Systems*, vol. 19, no. 3-4, pp. 223–249, 2005.

[14] Z.-L. Li, R. Tang, Z. Wan et al., "A review of current methodologies for regional evapotranspiration estimation from remotely sensed data," *Sensors*, vol. 9, no. 5, pp. 3801–3853, 2009.

[15] L. Jiang and S. Islam, "A methodology for estimation of surface evapotranspiration over large areas using remote sensing observations," *Geophysical Research Letters*, vol. 26, no. 17, pp. 2773–2776, 1999.

[16] L. Jiang and S. Islam, "Estimation of surface evaporation map over southern Great Plains using remote sensing data," *Water Resources Research*, vol. 37, no. 2, pp. 329–340, 2001.

[17] T. Carlson, "An overview of the 'triangle method' for estimating surface evapotranspiration and soil moisture from satellite imagery," *Sensors*, vol. 7, no. 8, pp. 1612–1629, 2007.

[18] G. J. Roerink, Z. Su, and M. Menenti, "S-SEBI: a simple remote sensing algorithm to estimate the surface energy balance," *Physics and Chemistry of the Earth, Part B: Hydrology, Oceans and Atmosphere*, vol. 25, no. 2, pp. 147–157, 2000.

[19] Z. Su, "The Surface Energy Balance System (SEBS) for estimation of turbulent heat fluxes," *Hydrology and Earth System Sciences*, vol. 6, no. 1, pp. 85–99, 2002.

[20] G. Y. Qiu, T. Yano, and K. Momii, "Estimation of plant transpiration by imitation leaf temperature. I. Theoretical consideration and field verification," *Transaction of the Japanese Society of Irrigation, Drainage and Reclamation Engineering*, vol. 64, pp. 401–410, 1996.

[21] G. Y. Qiu, T. Yano, and K. Momii, "An improved methodology to measure evaporation from bare soil based on comparison of surface temperature with a dry soil," *Journal of Hydrology*, vol. 210, no. 1–4, pp. 93–105, 1998.

[22] Y. J. Xiong and G. Y. Qiu, "Estimation of evapotranspiration using remotely sensed land surface temperature and the revised three-temperature model," *International Journal of Remote Sensing*, vol. 32, no. 20, pp. 5853–5874, 2011.

[23] Q. Mu, F. A. Heinsch, M. Zhao, and S. W. Running, "Development of a global evapotranspiration algorithm based on MODIS and global meteorology data," *Remote Sensing of Environment*, vol. 111, no. 4, pp. 519–536, 2007.

[24] Q. Mu, M. Zhao, and S. W. Running, "Improvements to a MODIS global terrestrial evapotranspiration algorithm," *Remote Sensing of Environment*, vol. 115, no. 8, pp. 1781–1800, 2011.

[25] K. Zhang, J. S. Kimball, R. R. Nemani, and S. W. Running, "A continuous satellite-derived global record of land surface evapotranspiration from 1983 to 2006," *Water Resources Research*, vol. 46, no. 9, Article ID W09522, 2010.

[26] R. Leuning, Y. Q. Zhang, A. Rajaud, H. Cleugh, and K. Tu, "A simple surface conductance model to estimate regional evaporation using MODIS leaf area index and the Penman-Monteith equation," *Water Resources Research*, vol. 44, no. 10, Article ID W10419, 2008.

[27] L. Jia, Z. Su, B. van den Hurk et al., "Estimation of sensible heat flux using the Surface Energy Balance System (SEBS) and ATSR measurements," *Physics and Chemistry of the Earth*, vol. 28, no. 1–3, pp. 75–88, 2003.

[28] W. W. Verstraeten, F. Veroustraete, and J. Feyen, "Estimating evapotranspiration of European forests from NOAA-imagery at satellite overpass time: towards an operational processing chain for integrated optical and thermal sensor data products," *Remote Sensing of Environment*, vol. 96, no. 2, pp. 256–276, 2005.

[29] R. K. Singh, A. Irmak, S. Irmak, and D. L. Martin, "Application of SEBAL model for mapping evapotranspiration and estimating surface energy fluxes in South-Central Nebraska," *Journal of Irrigation and Drainage Engineering*, vol. 134, no. 3, pp. 273–285, 2008.

[30] F. Tian, G. Qiu, Y. Yang, Y. Lü, and Y. Xiong, "Estimation of evapotranspiration and its partition based on an extended three-temperature model and MODIS products," *Journal of Hydrology*, vol. 498, pp. 210–220, 2013.

[31] X. Zhao and Y. Liu, "Relative contribution of the topographic influence on the triangle approach for evapotranspiration estimation over mountainous areas," *Advances in Meteorology*, vol. 2014, Article ID 584040, 16 pages, 2014.

[32] J. D. Kalma, T. R. McVicar, and M. F. McCabe, "Estimating land surface evaporation: a review of methods using remotely sensed surface temperature data," *Surveys in Geophysics*, vol. 29, no. 4-5, pp. 421–469, 2008.

[33] Z. Jia, S. Liu, D. Mao, Z. Wang, Z. Xu, and R. Zhang, "A study of the validation method of remotely sensed evapotranspiration based on observation data," *Advances in Earth Science*, vol. 11, pp. 1248–1260, 2010.

[34] R. R. Gillies, W. P. Kustas, and K. S. Humes, "A verification of the 'triangle' method for obtaining surface soil water content energy fluxes from remote measurements of the normalized difference vegetation index (NDVI) and surface radiant temperature," *International Journal of Remote Sensing*, vol. 18, no. 15, pp. 3145–3166, 1997.

[35] Y. Liu, T. Hiyama, T. Yasunari, and H. Tanaka, "A nonparametric approach to estimating terrestrial evaporation: validation in eddy covariance sites," *Agricultural and Forest Meteorology*, vol. 157, pp. 49–59, 2012.

[36] G. Bisht, V. Venturini, S. Islam, and L. Jiang, "Estimation of the net radiation using MODIS (Moderate Resolution Imaging Spectroradiometer) data for clear sky days," *Remote Sensing of Environment*, vol. 97, no. 1, pp. 52–67, 2005.

[37] S. Liang, A. H. Strahler, and C. Walthall, "Retrieval of land surface albedo from satellite observations: a simulation study," *Journal of Applied Meteorology*, vol. 38, no. 6, pp. 712–725, 1999.

[38] M. S. Moran, R. D. Jackson, L. H. Raymond, L. W. Gay, and P. N. Slater, "Mapping surface energy balance components by combining Landsat Thematic Mapper and ground-based meteorological data," *Remote Sensing of Environment*, vol. 30, no. 1, pp. 77–87, 1989.

[39] K. Wilson, A. Goldstein, E. Falge et al., "Energy balance closure at FLUXNET sites," *Agricultural and Forest Meteorology*, vol. 113, no. 1–4, pp. 223–243, 2002.

[40] T. Foken, "The energy balance closure problem: an overview," *Ecological Applications*, vol. 18, no. 6, pp. 1351–1367, 2008.

[41] M. Mauder, C. Liebethal, M. Göckede, J.-P. Leps, F. Beyrich, and T. Foken, "Processing and quality control of flux data during LITFASS-2003," *Boundary-Layer Meteorology*, vol. 121, no. 1, pp. 67–88, 2006.

[42] M. Mauder, S. P. Oncley, R. Vogt et al., "The energy balance experiment EBEX-2000. Part II: intercomparison of eddy-covariance sensors and post-field data processing methods," *Boundary-Layer Meteorology*, vol. 123, no. 1, pp. 29–54, 2007.

[43] Z. Xu, S. Liu, X. Li et al., "Intercomparison of surface energy flux measurement systems used during the HiWATER-MUSOEXE," *Journal of Geophysical Research Atmospheres*, vol. 118, no. 23, pp. 13140–13157, 2013.

[44] P. Schotanus, F. T. M. Nieuwstadt, and H. A. R. De Bruin, "Temperature measurement with a sonic anemometer and its application to heat and moisture fluxes," *Boundary-Layer Meteorology*, vol. 26, no. 1, pp. 81–93, 1983.

[45] R. G. Allen, L. S. Pereira, T. A. Howell, and M. E. Jensen, "Evapotranspiration information reporting: I. Factors governing measurement accuracy," *Agricultural Water Management*, vol. 98, no. 6, pp. 899–920, 2011.

[46] G. L. Squires, *Practical Physics*, Cambridge University Press, Cambridge, UK, 2001.

[47] J. R. Nagol, E. F. Vermote, and S. D. Prince, "Effects of atmospheric variation on AVHRR NDVI data," *Remote Sensing of Environment*, vol. 113, no. 2, pp. 392–397, 2009.

[48] Z. Jia, S. Liu, Z. Xu, Y. Chen, and M. Zhu, "Validation of remotely sensed evapotranspiration over the Hai River Basin, China," *Journal of Geophysical Research: Atmospheres*, vol. 117, no. 13, 2012.

[49] X. Li, G. Cheng, S. Liu et al., "Heihe watershed allied telemetry experimental research (HiWATER): scientific objectives and experimental design," *Bulletin of the American Meteorological Society*, vol. 94, pp. 1145–1160, 2013.

[50] J. Wang, J. Zhuang, W. Wang, S. Liu, and Z. Xu, "Assessment of uncertainties in eddy covariance flux measurement based on intensive flux matrix of HiWATER-MUSOEXE," *IEEE Geoscience and Remote Sensing Letters*, vol. 12, no. 2, pp. 259–263, 2015.

[51] S. M. Liu, Z. W. Xu, W. Z. Wang et al., "A comparison of eddy-covariance and large aperture scintillometer measurements with respect to the energy balance closure problem," *Hydrology and Earth System Sciences*, vol. 15, no. 4, pp. 1291–1306, 2011.

[52] A. Savtchenko, D. Ouzounov, S. Ahmad et al., "Terra and Aqua MODIS products available from NASA GES DAAC," *Advances in Space Research*, vol. 34, no. 4, pp. 710–714, 2004.

[53] W. P. Menzel, S. W. Seemann, J. Li, and L. E. Gumley, "MODIS atmospheric profile retrieval algorithm theoretical basis document," Version 6, Reference Number: ATBD-MOD-07, http://modis.gsfc.nasa.gov/data/atbd/atbd_mod07.pdf.

[54] Z. Wan and J. Dozier, "A generalized split-window algorithm for retrieving land-surface temperature from space," *IEEE Transactions on Geoscience and Remote Sensing*, vol. 34, no. 4, pp. 892–905, 1996.

[55] A. Huete, K. Didan, T. Miura, E. P. Rodriguez, X. Gao, and L. G. Ferreira, "Overview of the radiometric and biophysical performance of the MODIS vegetation indices," *Remote Sensing of Environment*, vol. 83, no. 1-2, pp. 195–213, 2002.

[56] A. R. Huete, K. Didan, Y. E. Shimabukuro et al., "Amazon rainforests green-up with sunlight in dry season," *Geophysical Research Letters*, vol. 33, no. 6, Article ID L06405, 2006.

[57] C. B. Schaaf, F. Gao, A. H. Strahler et al., "First operational BRDF, albedo nadir reflectance product from MODIS," *Remote Sensing of Environment*, vol. 83, pp. 135–148, 2003.

[58] J. G. Salomon, C. B. Schaaf, A. H. Strahler, F. Gao, and Y. Jin, "Validation of the MODIS Bidirectional Reflectance Distribution Function and albedo retrievals using combined observations from the Aqua and Terra platforms," *IEEE Transactions on Geoscience and Remote Sensing*, vol. 44, no. 6, pp. 1555–1564, 2006.

[59] Y. Yamaguchi, A. B. Kahle, H. Tsu, T. Kawakami, and M. Pniel, "Overview of advanced space-borne thermal emission and reflection radiometer (ASTER)," *IEEE Transactions on Geoscience and Remote Sensing*, vol. 36, no. 4, pp. 1062–1071, 1998.

[60] A. Gillespie, S. Rokugawa, T. Matsunaga, J. S. Cothern, S. Hook, and A. B. Kahle, "A temperature and emissivity separation algorithm for Advanced Spaceborne Thermal Emission and Reflection Radiometer (ASTER) images," *IEEE Transactions on Geoscience and Remote Sensing*, vol. 36, no. 4, pp. 1113–1126, 1998.

[61] H. Li, D. Sun, Y. Yu et al., "Evaluation of the VIIRS and MODIS LST products in an arid area of Northwest China," *Remote Sensing of Environment*, vol. 142, pp. 111–121, 2014.

[62] H. Li, H. S. Wang, Y. M. Du, Q. Xiao, and Q. H. Liu, "HiWATER: ASTER LST and LSE dataset in 2012 in the middle reaches of the Heihe River Basin," *Cold and Arid Regions Science Data Center at Lanzhou*, 2015.

[63] J. Cheng, S. Liang, Y. Yao, and X. Zhang, "Estimating the optimal broadband emissivity spectral range for calculating surface

longwave net radiation," *IEEE Geoscience and Remote Sensing Letters*, vol. 10, no. 2, pp. 401–405, 2013.

[64] J. C. Jiménez-Muñoz and J. A. Sobrino, "A generalized single-channel method for retrieving land surface temperature from remote sensing data," *Journal of Geophysical Research: Atmospheres*, vol. 108, p. D22, 2003.

[65] G. Bisht and R. L. Bras, "Estimation of net radiation from the MODIS data under all sky conditions: Southern Great Plains case study," *Remote Sensing of Environment*, vol. 114, no. 7, pp. 1522–1534, 2010.

[66] B. A. Wielicki, B. R. Barkstrom, E. F. Harrison, R. B. Lee III, G. Louis Smith, and J. E. Cooper, "Clouds and the Earth's Radiant Energy System (CERES): an earth observing system experiment," *Bulletin of the American Meteorological Society*, vol. 77, no. 5, pp. 853–868, 1996.

[67] Atmospheric Science Data Center, *CERES Aqua Edition3A SSF Surface Fluxes—Accuracy and Validation*, 2010, https://eosweb.larc.nasa.gov/sites/default/files/project/ceres/quality_summaries/ssf_surface_flux_aqua_ed3A.pdf.

[68] X. Pan, Y. Liu, and X. Fan, "Comparative assessment of satellite-retrieved surface net radiation: an examination on CERES and SRB datasets in China," *Remote Sensing*, vol. 7, no. 4, pp. 4899–4918, 2015.

[69] M. J. Suarez, M. M. Rienecker, R. Todling et al., *The GEOS-5 Data Assimilation System-Documentation of Versions 5.0. 1, 5.1. 0, and 5.2. 0*, vol. 27 of *Technical Report Series on Global Modeling and Data Assimilation*, NASA, 2008.

[70] Z. Wan, Y. Zhang, Q. Zhang, and Z.-L. Li, "Validation of the land-surface temperature products retrieved from terra moderate resolution imaging spectroradiometer data," *Remote Sensing of Environment*, vol. 83, no. 1-2, pp. 163–180, 2002.

[71] G. Hulley, S. Veraverbeke, and S. Hook, "Thermal-based techniques for land cover change detection using a new dynamic MODIS multispectral emissivity product (MOD21)," *Remote Sensing of Environment*, vol. 140, pp. 755–765, 2014.

[72] Z. Jiao, H. Zhang, Y. Dong, Q. Liu, Q. Xiao, and X. Li, "An algorithm for retrieval of surface albedo from small view-angle airborne observations through the use of BRDF archetypes as prior knowledge," *IEEE Journal of Selected Topics in Applied Earth Observations and Remote Sensing*, vol. 8, no. 7, pp. 3279–3293, 2015.

[73] J. Li, Y. L. Zeng, Q. H. Liu, B. Zhong, S. L. Wu, and J. J. Peng, *1km NDVI Dataset in China and ASEAN (2013) (MuSyQ-NDVI-1km-2013)*, Global Change Research Data Publisher and Repository, 2015.

[74] B. Zhong, S. L. Wu, Q. H. Liu, X. J. Shan, A. X. Yang, and J. J. Peng, "1 km and 5 daily surface albedo dataset in China and ASEAN, 2013, (MuSyQ-REF-1 km-, 2013)," *Global Change Research Data Publisher and Repository*, 2015.

[75] X. Zhao, Y. Liu, D. Zhao, and J. Peng, "Estimating evapotranspiration using triangle method with topographic correction from MODIS data in Taihu Basin, China," in *Proceedings of the 6th International Conference on Wireless Communications Networking and Mobile Computing (WiCOM '10)*, pp. 1–5, IEEE, Chengdu City, China, September 2010.